Supplement of Atmos. Chem. Phys., 26, 4067–4088, 2026
https://doi.org/10.5194/acp-26-4067-2026-supplement

Atmospheric Chemistry and Physics
Open Access
EGU

Supplement of

Drop clustering and drop size correlations from holographic imagery suggest cloud droplet spectral broadening via entrainment-mixing

John J. D'Alessandro et al.

Correspondence to: John J. D'Alessandro (john.d-alessandro@univ-lille.fr)

Supplementary material

Part I:

In this section, we will evaluate an example of biases associated with diagnosing a system of droplets. Specifically, we explore whether drop sizes – DCF relationships can be diagnosed by simply applying the RDF equation (eq. 1). This bias will be demonstrated in the context of evaluating DCFs for separate drop size ranges (drops having D<25 µm and D>25 µm). First, we must alter the RDF equation to compute a partial RDF, such that

$$g_{Drange}(r) = \sum_{i=1}^{N_{Drange}} \frac{\psi_i(r)/N_{Drange}}{(N-1)\left(\frac{dV_r}{V}\right)}$$

where $\psi(r)$ is the number of particles surrounding the *i*th particle within the surrounding spherical shell volume between radii $r - \Delta r/2$ and $r + \Delta r/2$, V is the measurement volume over the entire hologram, N is the number of drops within the guardrails and dV_r is the measurement volume enclosed within shells having radii $r - \Delta r/2$ and $r + \Delta r/2$. The only new variable is N_{Drange}, which is the concentration of drops within a given size range.

Figure S1 below shows the g_{Drange} for drops with diameters less than 25 µm (red lines) and greater than 25 µm (blue lines). Results are only shown for flight leg RF10B (Table 1 in manuscript). The thick dark red and dark blue lines are the averages of all individual holograms' g_{Drange}, whereas semi-transparent red and blue lines are partial RDFs of individual holograms. Results are restricted to holograms containing drops with diameters (*D)* greater than and less than 25 µm.

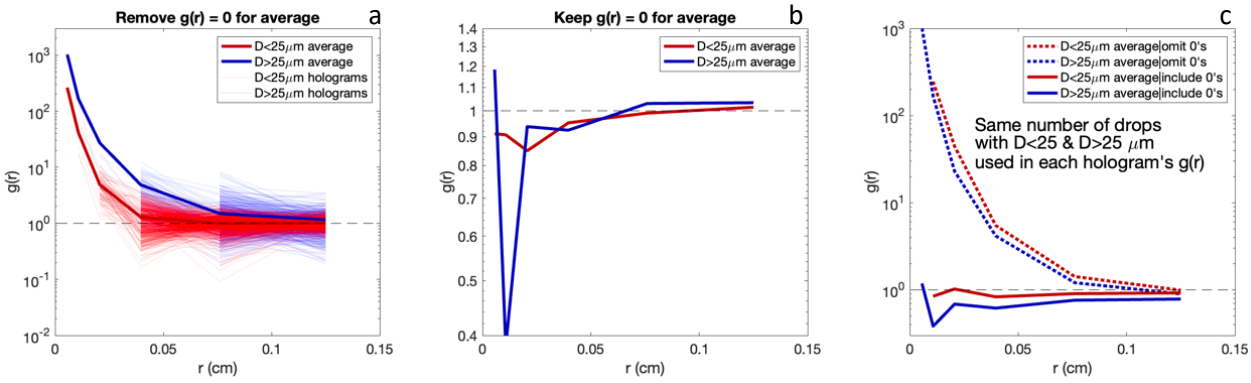

Figure S1: Partial RDFs computed over the second flight leg from RF10 (RF10B; Table 1) separately for drops with *D*<25 µm (red lines) and *D*>25 µm (blue lines). A) Partial RDFs are computed where the radial distance bins (r bins) having *g(r)* = 0 are omitted when averages are computed (thick lines). B) Average partial RDFs are computed where averages include radial distance values having *g(r)* = 0. C) Average partial RDFs similar to A and B, but are only computed for the same number of drops with *D*>25 µm and *D*<25 µm. Drops for the *D* range with the greater concentration are randomly selected to be the same number of drops for the *D* range with the lower concentration. Solid (dashed) lines correspond with average partial RDFs which include (omit) *g*(*r*) = 0 bins when computing averages.

Figure S1a shows partial RDFs computed for drops having D>25 μm (blue lines) and D<25 μm (red lines), and averages for the respective drop size ranges are denoted by the thick, darkly shaded lines. Partial RDFs with g(r) approaching one is indicative of Poisson (randomly) distributed droplets, and greater (lower) values indicate whether more (less) droplets are observed at the given r distance. In contrast to the manuscript finding large drops are likely isolated, Figure S1a indicates large drops are *more* likely to be in close proximity to surrounding drops compared with smaller drops (the red line is higher than the blue line). However, the characteristic inverse exponential shape of the RDFs results from ignoring r bins where g(r) = 0. Figure S1b only shows the average partial RDFs of the two drop size ranges similar to S1a, except r bins with g(r)=0 are included in the averaging. Note that these results have averages centered at g(r) = 1 at the larger r bins similar to S1a (r > ~0.75 cm), but now g(r) decreases below 1 at small r bins.

This is due to counting statistical uncertainties. Namely, when there are no pairs counted (Ψ=0), the expression may arguably be invalid since there is no data to be weighted by the denominator. This can be conceptually understood if we were to compute an RDF for droplets within a very small sample volume (e.g., our HOLODEC measurements of a few cubic centimeters) compared with a very large volume (e.g., much greater than a few cubic centimeters), where the latter will have a larger sample size of droplets and a greater likelihood of detecting droplet pairs at very close proximities to each other (i.e., very small r bins). This is particularly important to consider when exploring clustering characteristics at smaller spatial scales explored here (mm) than those where such biases are less likely to occur (cm).

It is also for this reason that Figure S1a&b show small droplets are more likely to be isolated from other drops than larger drops (blue lines above red lines). This is because there is usually a greater number of drops with D < 25 μm than drops with D > 25 μm, and this consequentially produces a greater number of g(r) = 0 to be included in the averages for D > 25 μm. To highlight this, Figure S1c shows average partial RDFs of the two drop size ranges but it is only computed for the same number of available drops for each hologram. Because there are usually more small drops than larger drops, partial RDFs are generally computed for a reduced number of small drops equaling the number of large drops. Average partial RDFs are shown when omitting g(r) = 0 bins (dashed lines) and including g(r) = 0 bins (solid lines) in the calculation. We see for both sets of average RDFs that the large drops are now more isolated than smaller drops (red lines above the blue lines).

Now that we have potentially captured a similar trend as in our paper, it follows that we would want to determine the statistical significance of these partial RDFs. However, there is no universally accepted method to do so. Previous studies have simulated Poisson distributed environments of droplets (Larsen and Shaw, 2018) or used a simple ad hoc methodology (Larsen et al., 2018).

To conclude: we showed 1) that large drops can be shown to be more isolated than small drops using partial RDFs and 2) how statistical counting uncertainties can introduce errors into our outputs. However, our proposed methodology avoids these counting uncertainties by determining the likelihoods drops of a given size range will be 1) isolated or 2) have a high number of neighboring drops by randomly shuffling the drop sizes within the respective holograms while keeping the droplet spatial coordinates unchanged. Our methodology also tests for statistical significance whereas there is some ambiguity of how to best determine uncertainty for partial RDF computations.

Part II:

Results here primarily focus on sensitivity tests of the "large drop isolation trend", which are shown in Table S1. Results from one sensitivity test are shown in Figure S3 (dependence on drop size threshold). Additional sensitivity tests are available upon request.

<table>
<tr><th colspan="8">Sensitivity Tests</th></tr>
<tr><th>Sensitivity test</th><th colspan="6">Conditions</th><th>Rationale/discussion</th></tr>
<tr><td rowspan="3">Test alternative version of Table 3 with slightly different thresholds</td><td>N</td><td><100</td><td>100–170</td><td>170–240</td><td>240–300</td><td>>300</td><td rowspan="3">Results are consistent with original Table 3. However, note conditions at low drop concentrations are approximately similar, where the isolated large drop trend is observed.</td></tr>
<tr><td>Min ψ for high DCF</td><td>2</td><td>3</td><td>4</td><td>5</td><td>6</td></tr>
<tr><td>Min shell size for low DCF</td><td>r_{min}+ δr= 0.12 cm</td><td>r_{min}+ δr= 0.1 cm</td><td>r_{min}+ δr= 0.09 cm</td><td>r_{min}+ δr= 0.09 cm</td><td>r_{min}+ δr= 0.09 cm</td></tr>
<tr><td>Test larger shell sizes</td><td colspan="6">r_{min}+ δr=16cm, 17cm</td><td>-</td></tr>
<tr><td>Test for consideration of different small drop size threshold</td><td colspan="6">D=6 µm, 10 µm, 14 µm</td><td>- The HOLODEC detects drops as small as D=6 µm, but has improved detection for D>10 µm (references therein)</td></tr>
<tr><td rowspan="2">Test DCF>67th percentile for Monte Carlo – Hologram Comparisons</td><td>Categories</td><td colspan="2">HILD</td><td colspan="2">OTHER</td><td rowspan="2">-</td></tr>
<tr><td>Percentiles</td><td colspan="2">D: 25-30 µm > 95th
D: 30-37.5 µm > 95th
D: 37.5-50 µm > 90th</td><td colspan="2">D: 25-30 µm < 85th
D: 30-37.5 µm < 85th
D: 37.5-50 µm < 85th</td></tr>
<tr><td>Adjust $N_{DCF\_category}$ lower bound</td><td colspan="6">Tested possibilities of $N_{DCF\_category}$ threshold of 1,2,…,10</td><td>Results are consistent for $N_{DCF\_category}$ = 2–10</td></tr>
<tr><td rowspan="2">Extend HOLODEC sample volume</td><td colspan="3">Inner sample volume dimensions</td><td colspan="3">Guard rail dimensions</td><td rowspan="2">-</td></tr>
<tr><td colspan="3">0.7 cm × 0.7 cm × 10.1 cm</td><td colspan="3">0.4 cm × 0.4 cm × 9.8 cm</td></tr>
</table>

Table S1: List of sensitivity tests.

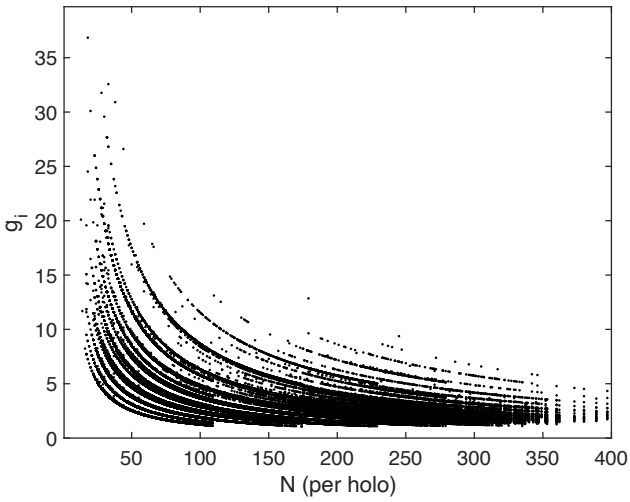

Figure S2: Plot of hologram drop concentration (per sample volume) related to g_i (Eq. 2). All drops used in the analysis as defined in Sections 2 and 3 are included here. Note that only the maximum g_i are shown amongst all shell sizes for a given drop, and a minimum number of neighboring drops is required for a given drop concentration. This is what produces characteristic cut-offs in the datapoints at N=110, 175, etc., which correspond to drop concentration thresholds in Step 3 of Table 2.

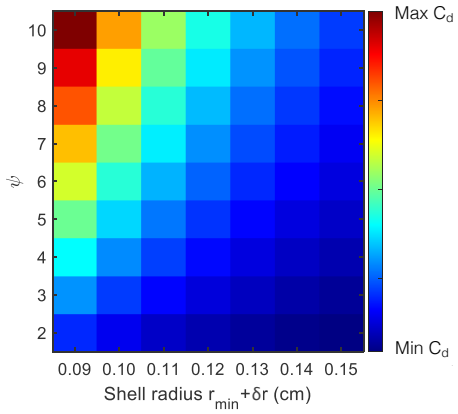

Figure S3: Ranked C_d for varying shell sizes and number of drops within the respective shells.

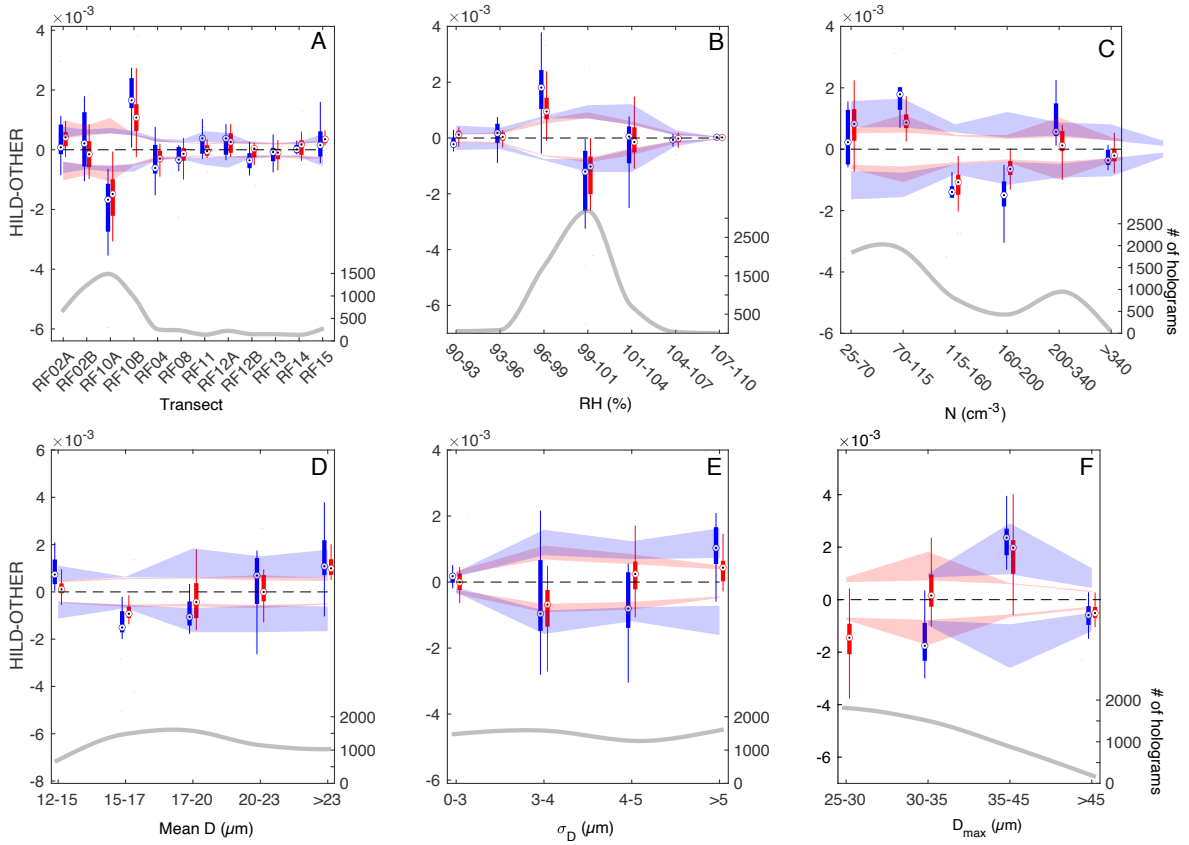

Figure S4: Identical to Figure 7, but using data from all flight legs in Table 1 and not just RF02A,B and RF10A,B.

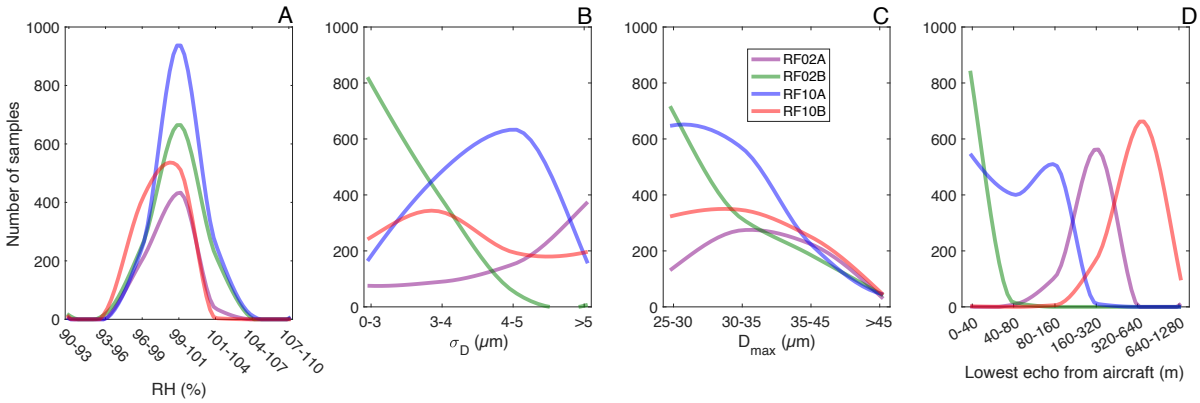

Figure S5: Histograms of *RH* (A), σ_D (B), D_{max} (C), and lowest detected cloud condensate (D) from the four flight legs evaluated in Section 4.2 (colored lines). Results in D) are reported as absolute distance from the aircraft, whereas the corresponding plot in Figure 8D ranks these values over each respective flight leg. A cubic interpolation is applied to the histograms.

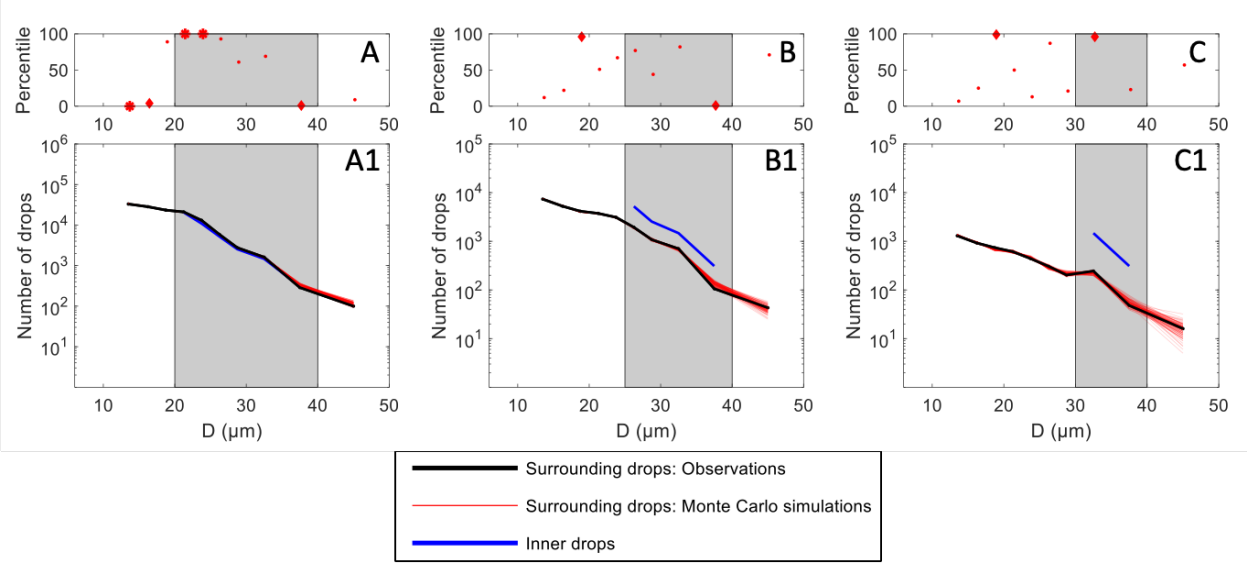

Figure S6: Plots showing percentiles (i.e., likelihoods) that drops of varying sizes will neighbor drops having diameters between 20–40 μm (A), 25–40 μm (B) and 30–40 μm (C). Frequency distributions of the neighboring drops (black lines) and the respective drop ranges (blue lines) are shown in A1, B1 and C1. Drops within these size ranges are termed inner drops. Results from neighboring drops are only shown for high DCF, and from the shell sizes which correspond to those of the maximum g_{drop}. Percentiles are computed similarly to the Monte Carlo-DCF methodology, whose simulated frequency distributions are shown by the thin red lines in A1, B1 and C1. Shaded regions correspond to the inner drops' size range.

Greater likelihoods of drops neighboring similarly sized drops are highlighted here, most notably for drops with diameters from 20–40 μm (S2A), where the highest likelihoods peak at drop sizes closest to D=20 μm (having the greatest occurrence frequencies amongst the size range).

Bibliography

Larsen, M. L. and Shaw, R. A.: A method for computing the three-dimensional radial distribution function of cloud particles from holographic images, Atmospheric Measurement Techniques, 11, 4261–4272, https://doi.org/10.5194/amt-11-4261-2018, 2018.

Larsen, M. L., Shaw, R. A., Kostinski, A. B., and Glienke, S.: Fine-Scale Droplet Clustering in Atmospheric Clouds: 3D Radial Distribution Function from Airborne Digital Holography, Phys. Rev. Lett., 121, 204501, https://doi.org/10.1103/PhysRevLett.121.204501, 2018.